Sub-micron lateral topography affects endothelial migration by modulation of focal adhesion dynamics

S Antonini[1], S Meucci[1,2], E Jacchetti[1], M Klingauf[2,3], F Beltram[1], D Poulikakos[3], M Cecchini[1] and A Ferrari[3]

[1] NEST, Istituto Nanoscienze-CNR and Scuola Normale Superiore, Piazza San Silvestro, 12, I-56126 Pisa, Italy
[2] Center for Nanotechnology Innovation @ NEST, Istituto Italiano di Tecnologia, Piazza San Silvestro 12, I-56127 Pisa, Italy
[3] Laboratory of Thermodynamics in Emerging Technologies, Department of Mechanical and Process Engineering, ETH Zurich, Sonneggstrasse 3, ML J 27.1, CH-8092 Zurich, Switzerland

E-mail: marco.cecchini@nano.cnr.it

RECEIVED
30 March 2015

REVISED
29 April 2015

ACCEPTED FOR PUBLICATION
26 May 2015

PUBLISHED
24 June 2015

Introduction

The endothelium lies at the blood–tissue interface of mammalian vessels [1]. It regulates body homeostasis by controlling transport phenomena between the bloodstream and surrounding tissues [2], the exchange of gas and nutrients, and transmural movement of effector cells [3]. A differentiated endothelium is composed by a confluent, growth-arrested monolayer of endothelial cells (ECs) that polarize in response to mechanical and chemical stimuli, and interact with a topographically structured basal matrix [4, 5]. The basal matrix is organized in a highly ordered pattern consisting of proteins bundled in quasi-parallel micron and submicron-sized fibers [6]. The interaction between ECs and the basal matrix is critical to endothelium functions in physiological and pathological processes. It is regulated both by the biochemical identity of the matrix proteins and by the matrix physical and mechanical properties [7]. Exploiting nano- and micro-engineered substrates it is possible to investigate the complex interaction between the basal matrix and the endothelium [8–10]. In fact this technological approach makes it possible to isolate the individual substrate properties that are actively sensed by ECs [4] such as the molecular composition of the local matrix, the adhesive ligand density, the surface substrate stiffness and topography [4, 6, 11].

The cellular machinery that mediates the recognition of topographical elements in the basal matrix is the focal adhesion. It assembles upon the local clustering of a sufficient number of integrin receptors in correspondence of specific matrix ligands [12]. Integrin binding fosters the recruitment of a number of signaling and adaptor proteins, e.g. focal adhesion kinase (FAK) and paxillin, at the cytoplasmic site of the adhesion (i.e. the adhesion plaque), along with a maturation process which eventually connects the adhesion plaque to the actin cytoskeleton thus allowing force to be exerted on the substrate via acto-myosin-mediated cell contractility [13, 14]. As a consequence, the signaling activity triggered by the adhesion assembly regulates cell sensing, shape, and contractility both via the interaction with the cell cytoskeleton and via a direct modulation of gene expression. Among the signaling molecules that are rapidly recruited at the adhesion plaque, FAK, an essential non-receptor tyrosine kinase, plays pivotal roles in spreading, migratory responses, adhesive signaling, and mechanotrasduction [10, 13, 15].

FAs are structurally exposed to the process of maturation, through which they dynamically elongate in the direction opposite to the exerted force [4, 16]. The driving force for maturation can be externally applied [17] or directly produced by the cell contractile activity. The latter is orchestrated by the non-muscolar myosin-II and regulated via the Rho-ROCK pathway [18–20]. Topographical obstacles can interfere with FA maturation, forcing adhesion assembly in a preferential direction or hampering adhesion maturation [16, 21, 22]. In this way, topographical modifications of the substrate can be exploited to either favor or demote selected cell activities [11] including adhesion [23], migration [9, 24] and differentiation [25, 26]. Altogether, the cellular response to the local surface topography is identified as contact guidance [11].

Re-establishment of a functional tissue through the rapid coverage of target surfaces by ECs (i.e. the process of re-endothelialization) is required in order to avoid inflammatory or thrombogenic responses to implant materials which are in contact with the blood flow, e.g. stents or assisting devices [27]. Micron-sized gratings can contribute to re-endothelialization by favoring cell polarization and controlling their density and migration within the endothelium, thereby promoting the process of wound healing [10]. While several specific applications of surface texture were reported, a general understanding of the link between geometry of surface topography, FA maturation dynamics, and the resulting EC behavior is still missing. In this frame, the identification of the underlying mechanism is expected to pave the way to the generation of libraries of surface geometries which maximize endothelialization under specific conditions.

In this study, we analyze how the lateral feature size of gratings in the micron and submicron range affects human umbilical-vein endothelial cells (HUVECs) polarization and spreading, and controls FA maturation dynamics using a total internal reflection fluorescence (TIRF) microscope. We believe that this study improves the current understanding of the interaction between ECs and textured substrates, thus providing a useful reference for the rational engineering of surfaces aimed at promoting the rapid and functional coverage by endothelial cells.

Materials and methods

Substrate fabrication

The gratings were imprinted on 180 μm thick untreated cyclic olefin copolymer (COC) foils (Ibidi, Germany) using nanoimprint lithography as previously reported [16, 19, 28]. This procedure generated squared patterned areas of 4 mm side length. Molds were fabricated with a height of 400 nm and varying ridge and groove sizes (table 1). The COC substrates were placed on top of the mold and softened by raising the temperature up to 150 °C. A pressure of 50 bar was then applied for 10 min before cooling down to 40 °C. Finally, the pressure was released and the mold was detached from the substrate with a scalpel. Substrates were glued on the bottom of 35 mm tissue-culture dishes using a silicon rubber compound (RS 692-542). Glued substrates were incubated with 1.5% gelatin (DIFCO 214340) in dH_2O for 1 h at room temperature (RT). After removal gelatin was fixed using 2% glutaraldehyde in dH_2O for 15 min at RT. After fixation glutaraldehyde was exchanged with 70% ethanol in PBS and incubated for 60 min at RT. Next, gelatin-coated substrates were washed five times with PBS and placed under PBS containing 2 mM glycine overnight. Finally, samples were washed in sterile PBS and stored at 4 °C till seeding of HUVECs.

Table 1. Lateral features of the different nanogratings.

Designation	Ridge width	Groove width
T1	0.5 μm	0.5 μm
A1.5	1.0 μm	0.5 μm
A2.0	1.5 μm	0.5 μm
T2	1.0 μm	1.0 μm
T4	2.0 μm	2.0 μm

Cell culture and wound healing

HUVECs (Invitrogen) were seeded in T25 flasks coated with 1% gelatin, cultured in EGM-2-MV BulletKit (Lonza, Milano, Italy) complete medium, (i.e. EBM-2 medium supplemented with 10% FBS, Hydrocortisone 0,2 ml, hFGF-B 2 ml, VEGF 0,5 ml, R3-IGF-1 0,5 ml, Ascorbic Acid 0,5 ml, hEGF 0,5 ml, GA-1000 0,5 ml, Heparin 0,5 ml); the cells were maintained at 37 °C and 5% CO_2. All experiments were performed using cells with less than seven passages *in vitro*. To generate confluent monolayers, cells were seeded on COC substrates at high density (60–70 $\times$ 10^4 cells per cm^2) as reported by Lampugnani *et al* [29] and cultured for two days. After washing with medium cells were gently wounded by a plastic micropipette tip.

Antibodies, chemicals and constructs

Mouse anti-vinculin (V4505) and mouse anti-tubulin (T6074) were purchased from Sigma. Phalloidin-Alexa-647 (V22886) was purchased from Invitrogen. Secondary goat anti-mouse Alexa-488 was purchased from Sigma. Paxillin-EGFP was kindly provided by Juergen Wehland (Helmholtz Centre for Infection Research, Braunschweig, Germany).

HUVEC transfection and TIRF microscopy

For TIRF analysis, HUVECs were transfected with paxillin-EGFP (1 μg DNA / 150 000 cells) using a Neon Transfection System (Invitrogen; 1350 V, 1 pulse, 30 ms) and densely seeded. 24 h after transfection, transfected cells were analyzed using a TIRF system (AF6000) equipped with an incubation chamber where temperature and CO_2 concentration were maintained at 37 °C and 5%, respectively. Pictures were taken every minute for 45 min using a 63× objective and a penetration depth of 120 nm.

Wide-field microscopy

Wide-field images were recorded using a Nikon-Ti wide-field microscope (Nikon, Japan) equipped with an Orca R-2 CCD camera (Hamamatsu Photonics, Japan). Dishes containing the topographic chip were placed under the microscope in an incubated chamber (Life Imaging Services, Switzerland), where temperature and CO_2 concentration were maintained at 37 °C and 5%, respectively. Images were collected with a 20× 0.45 NA long-distance objective (Plan Fluor, Nikon). Cell spreading and alignment were recorded in living cells using the DIC channel.

Confocal microscopy

Fixed and stained HUVEC monolayers were recorded using a Leica SP2 AOBS microscope (Leica Microsystems) equipped with a 40× (1.25-0.75NA, Oil, HC Plan-Apo CS) objective and Ar (emission 488, detection 495–550 nm), He/Ne (emission 633, detection 650–800 nm) and UV (emission 405, detection 410–470 nm) lasers.

Single-cell and monolayer polarization analysis

Fiji (ImageJ) was used to manually detect ('Freehand selection' tool) single HUVEC in the DIC channel. The options 'Area' and 'Feret angle' of the 'Measurement' tool provided information on cell spreading and alignment to the underlying pattern. In particular, cell alignment was defined as the angle between the direction of major axis of each cell, measured as 'Feret's diameter', and the one of the grating. For monolayer alignment the option 'Directionality' of Fiji was used. This function calculates a directionality histogram by calculating the fast Fourier transform (FFT) of the analyzed image and measuring the intensity of the spectrum in each direction. The histogram was then fitted with a Gaussian curve which provided two information: the mean of the curve and its variance (s^2).

The first parameter was used to identify the direction in which the monolayer is oriented, and the second was used to represent the homogeneity of the cell-layer (low values of s^2 indicate high coherence of the monolayer).

TIRF image analysis

Movies of paxillin-transfected cells were processed using a Matlab script. For each movie image-intensity histograms were created. These usually displayed two peaks: a low-intensity one corresponding to the background and a higher-intensity one relative to the fluorescent emission. A threshold was therefore defined between the two peaks and the pixels were divided in two groups: background pixels and focal adhesion pixels. The first group was excluded from the analysis, the other one was used to calculate the oscillations of paxillin-GFP over time by estimating the standard deviation (SD) of the fluorescence of each pixel over time. Furthermore, the script recorded the time and duration in which the intensity of a pixel passed the threshold, called appearance time and lifetime, respectively.

Results

Influence of periodicity and duty cycle on individual EC spreading and alignment

The biocompatibility of cyclic olefin copolymer (COC) substrates interacting with HUVECs is well established [10, 16].

In order to evaluate the effect of the lateral feature size of anisotropic patterns, we generated a set of gratings with constant groove depth (0.4 μm) but variable periodicity (1–4 μm) and ridge size (0.5–2 μm, see table 1). The groove depth was chosen to match the average of values reported in previous studies [8–10, 16, 30, 31]. Additionally, 0.4 μm-deep gratings were shown to induce effective contact guidance on ECs [10] thus providing the best conditions to isolate the effect of lateral-feature size. We initially detected the response of individual ECs by measuring the cell area in contact with the underlying substrate (i.e. the spreading) and cell-body orientation. Figure 1(a) shows that spreading was significantly decreased with lower-periodicity substrates (T1) and reached 44.6 ± 5.0% of the basal area of cells in the case of control (FLAT) substrates. Cell spreading on gratings with increasing ridge width (from 0.5 to 2 μm) was similarly reduced when compared to the value measured on control substrates. Maximum spreading (75.5 ± 4.5% of FLAT control) was obtained with gratings with 1.5 μm ridge width and 2 μm lateral period. Interestingly, gratings with the same lateral period but 50% duty cycle (i.e. ridge width = groove width) (T2, table 1) proved ideal for ECs spreading (112.7 ± 13.8% of the FLAT control). A further increase of the lateral periodicity (T4, table 1) led to a reduction of cell spreading down to 78.7 ± 8.6% of the FLAT control (figure 1(a)). In all, these results demonstrate that, among the tested textured substrates, gratings with lateral period of 2 μm and 1 μm-wide ridges proved best for EC spreading.

We previously reported that the effect of topography on EC spreading and contact guidance are independent and can be fully decoupled [10]. Thus we investigated the effect of lateral periodicity and ridge-width also on EC alignment to grating lines (figure 1(b)). Fully-spread ECs on FLAT substrates displayed random alignment, leading to an average orientation angle (45.7 ± 1.4°). Interaction with anisotropic patterns narrowed the orientation distribution, resulting in an average alignment angle of 18.6 ± 3.8° on gratings with lateral periodicity of 1 μm (T1; table 1). Alignment to gratings featuring large ridge width and periodicity (T4) was less efficient (24.6 ± 2.5°) while, interestingly, the grating yielding the best spreading (T2) also induced quasi-maximal alignment (13.3 ± 0.3°).

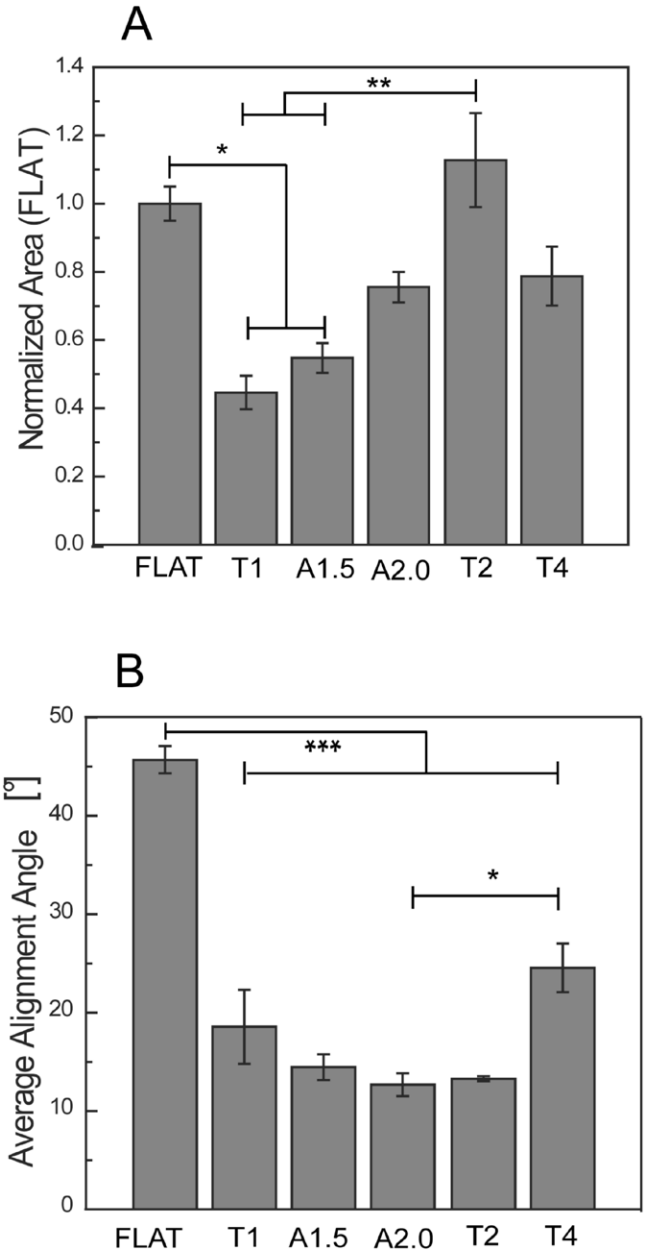

Figure 1. HUVEC alignment and spreading on patterned surfaces. Cells were seeded at low concentration on different gratings and analyzed by bright field microscopy. (A) Cell spreading area after 24 h. *$P < 0.05$ T1 versus FLAT, A1.5 versus FLAT and **$P < 0.01$ T1 versus T2, A1.5 versus T2 (One-Way ANOVA, Tukey's test). (B) Average cell alignment. *$P < 0.05$ A2.0 versus T4 and ***$P < 0.001$ each patterns versus FLAT (One-Way ANOVA, Tukey's test). Bars represent the mean of three independent experiments (40–50 cells each) ± SEM.

Effect on ECs in a monolayer

We next examined how anisotropic patterns affect ECs in growth-arrested endothelial monolayers. Here, cell polarity is revealed by the orientation of actin microfilaments and microtubules (figure 2). In control endothelia grown on FLAT substrates, cells showed a uniform angular distribution of actin and tubulin filaments. Gratings were efficient in significantly reducing the angular variance of filamentous actin, reaching the lowest value (corresponding to a maximum alignment; see Materials and Methods) of $s^2 = 40.2$ on gratings with lateral period of 2 μm and 50% duty cycle (T2; figure 2(a)). The alignment of microtubules showed a similar behavior for all tested substrates albeit with higher variance (figure 2(b)). High-resolution images of the cell cytoskeleton revealed that microtubules preferentially co-localized with ridges at the cell periphery (figure S1(a)) (stacks.iop.org/BMM/10/035010/mmedia). Actin microfibers were generally aligned along the gratings across the whole cell and did not show any preferred co-localization with ridges or grooves (figure S1(b)) (stacks.iop.org/BMM/10/035010/mmedia). In summary, the cytoskeleton of ECs aligned along the underlying pattern, with microfilaments being better oriented than microtubules. Additionally, pattern T2 (table 1) outperformed the other tested geometries in inducing the re-modeling and re-orientation of cytoskeletal components.

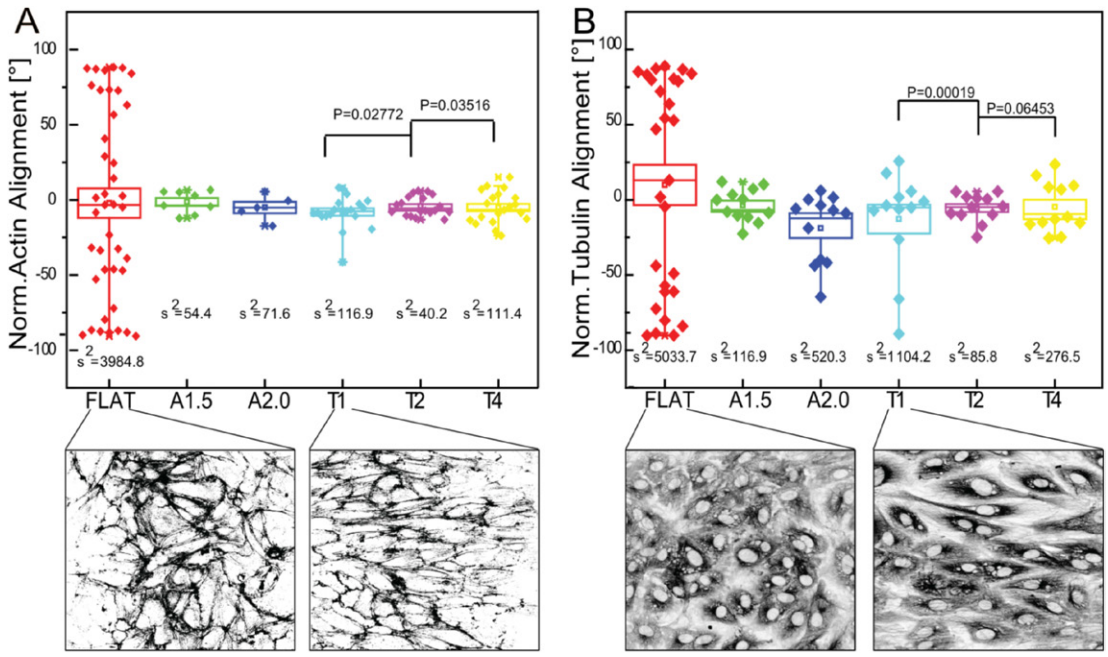

Figure 2. Alignment of HUVEC monolayers. HUVECs were grown into a monolayer, fixed and stained for actin and tubulin. For fluorescence images of fixed cells, a threshold was applied and analyzed by FFT for alignment, resulting in a directionality histogram. Graphs show deviation of directionality histogram peaks from the underlying pattern for actin (A) and tubulin (B), and representative images for T1 and FLAT. Three independent experiments were conducted (up to 15 fields of view per sample). Boxes represent SEM and whiskers 5–95 percentile. Means were tested using homogeneity of variance and analyzed using Levene's test.

FA stability is affected by grating periodicity

FAs act as sensors of substrate topography [16, 19, 32], and topographical features are known to interfere with the maturation of FAs [19]. The resulting dynamics of FA assembly and disassembly was linked to cell adhesion/migration [33, 34]. A high FA turnover is prevalent in migrating cells whereas stable adhesion are generally detected in fully spread, non-migrating cells [35].

In order to test if the gratings can affect FA dynamics in HUVECs, we visualized the paxillin-GFP signal in transfected ECs during wound healing. We restricted this analysis to T1, T2 (and FLAT) because they performed best among the tested gratings in inducing cell polarization and spreading. We previously established that fluorescently-labelled paxillin correctly localized to FAs and does not influence the migratory behavior [19]. FA dynamics was captured using a TIRF microscope. The resulting movies (a representative example is shown in supplementary movie 1) were analyzed to extract pixel-intensity dynamic lifetime (see Material and methods). Figure 3 provides an example of an EC migrating on grating T1. Here, pixels corresponding to the GFP signal at the cell-to-substrate interface were color-coded (figure 3(a)) to render the appearance time (lower left panel), lifetime (lower right panel), and dynamics (figure 3(b); see Material and methods) of the corresponding adhesions. This analysis was extended over all wound-healing movies and the resulting adhesion-lifetime and dynamic distributions are summarized in the scatter plots reported in figure 3(c). We focused on high- and middle-lifetime adhesions to avoid possible noise originating from fluorescence fluctuations and divided each lifetime-group according to the variation of the paxillin-GFP signal. The SD of pixel intensity over time indicates the molecular activity in the adhesion, and used to define three groups of pixels with increasing paxillin dynamics (low, medium and high SD), as shown by the scatter plot in figure 3(c). Figure 3(d) shows the relative difference from the values measured for ECs migrating on FLAT controls. Importantly, the fraction of high- and middle-lifetime adhesions was strongly reduced in cells migrating on grating T1 as compared to FLAT ($-86.7 \pm 6.1\%$ and $-68.7 \pm 4.7\%$; respectively). Interestingly, the FA lifetime in cells migrating on T2 gratings did not differ significantly from the FLAT control.

In summary, these data indicate that FAs formed in endothelial cells on gratings with lower periodicity (T1) are characterized by a slower turnover and an overall increased stability compared to ECs migrating on FLAT substrates or on gratings with larger ridges and grooves (T2).

Discussion

The investigation of the impact of specific topographical substrate modifications offers two main strategic advantages in the design and improvement of biomedical devices. Firstly, engineered surfaces were shown to strongly influence cell behavior upon adhesion. In particular, textured surfaces were successfully used to selectively populate target substrates with endothelial cells while demoting the adhesion and proliferation of smooth muscle cells [23], to instruct the commitment of stem cells [36],

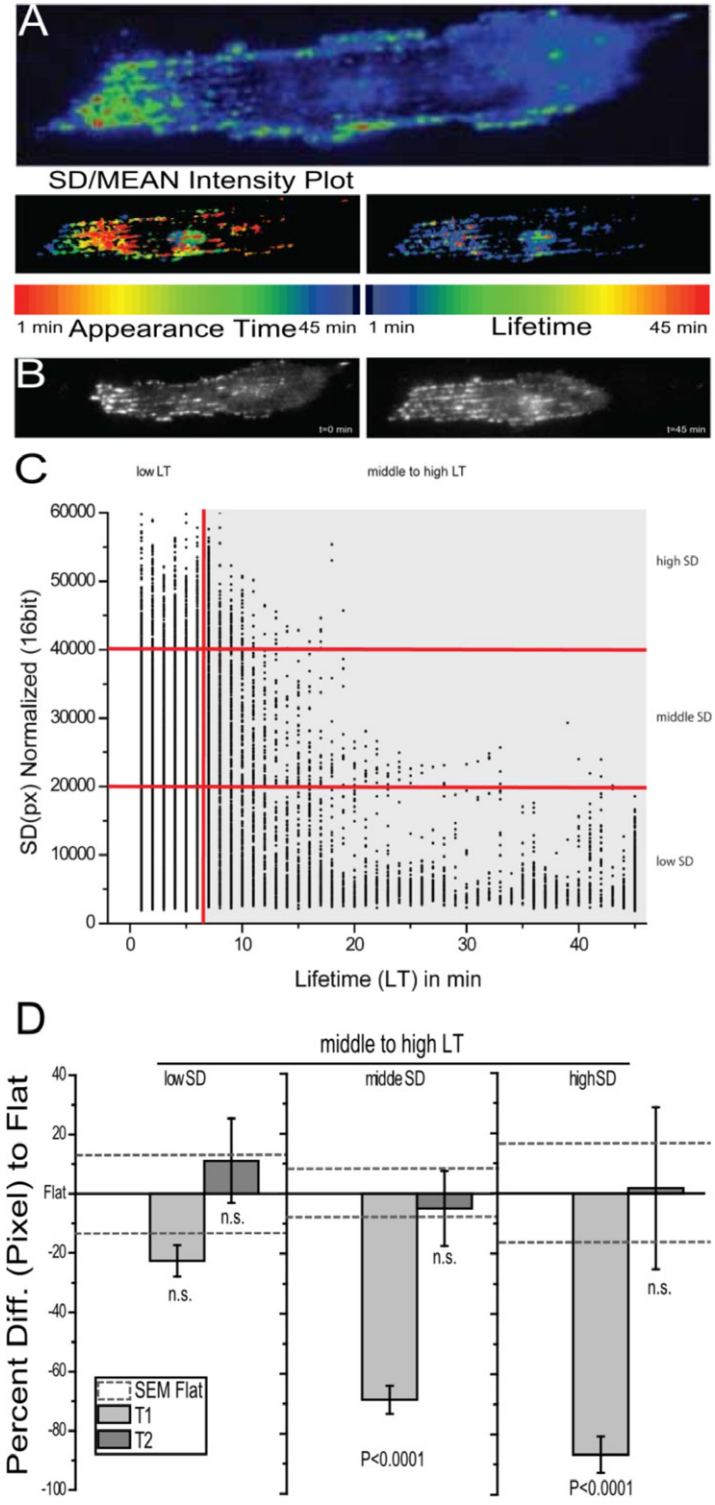

Figure 3. TIRF analysis of migrating paxillin-GFP expressing HUVECs. (A) Transfected cells at the wound edge were imaged in TIRF mode and paxillin-GFP signal was recorded vs time. The top panel shows the signal standard deviation (SD) of each pixel. The bottom panels show the appearance time (left, i.e. the time point when each pixel was brighter then threshold) and the lifetime of each pixel above threshold fluorescence (right). (B) SD appearance times at $t = 0$ min (left) and $t = 45$ min (right). (C) Scatter plot of normalized SD values versus lifetime of each pixel for one representative movie for the FLAT control. Plot was divided into 3 main areas corresponding to pixel high, middle or low SD, and middle to high lifetime. (D) Quantification of graph C. Ratios of the number of pixels with 'middle to high LT' over the ones with 'low LT' of each SD areas. Deviations from FLAT are shown as Mean ± SEM of 15–21 movies per condition. The Mann-Whitney test was used to assess significance.

to shape the function of polarized tissues [16], and/or to guide the movement of migrating cells [9]. The second fundamental asset involves the possibility of improving the performance of biomedical devices without modifying their overall macroscopic architecture or the chemical nature of the materials interfacing human tissues. This point is critical at the luminal surface of cardiovascular devices since inflammatory responses were shown to be induced by implanted materials.

The above considerations stimulated several studies empirically linking specific geometries and to characteristic cell responses. Unfortunately, these investigations are generally difficult to compare and can hardly lead to universal rules. A more useful approach may consist in dissecting the molecular mechanisms behind the recognition of surface topography and the effect of parametric variation of topographical features on cell machineries devoted to such processes [36]. In this direction we demonstrated how differentiating neurons can read nanoscopic variations in ridge width and respond by tuning both neuronal polarity and neurite alignment [16, 22, 37]. Similarly, we reported on how the vertical feature size promotes the spreading of endothelial cells [10]. In these reports we identified focal adhesion components as key players regulating surface recognition.

In this study, by using optically-accessible micropatterns, we investigated the effect of topography on focal adhesion dynamics in endothelial cells. Our data establish a link between the dynamic assembly/disassembly equilibrium of adhesions and the lateral feature size of gratings.

Notably, while a strong effect on cell polarization and alignment was evident on all tested anisotropic topographies (figures 1(b) and 2) it did not always translate into enhanced spreading (figure 1). Importantly, when investigating these cellular responses it is clear that textured substrates, as compared to their biochemically identical flat counterparts, generally yield a negligible or negative effect. In particular, cell spreading was hampered on most of the tested patterns (figure 1) indicating that the adhesion establishment and maturation are sub-optimal with such topographical features. Only in the case of gratings with specific lateral feature size (i.e. 1 μm) and duty cycle (i.e. 50%), a strong polarization of the cells is coupled with optimal spreading (figure 1).

These observations strongly suggest that contact guidance [38] and cell spreading [39] are not fully correlated cellular responses to substrate topography. Also based on previous literature [10], we speculate that the regulation of this outcome is determined by the dynamic equilibrium of focal-adhesion assembly and disassembly. While all gratings dictate the direction of focal-adhesion maturation and thus re-shape the cell cytoskeleton, only in cells interacting with 1 μm-wide ridges and grooves, this re-orientation yields efficient adhesion maturation, and, as a consequence, maximal spreading. Similarly, gratings strongly orient migration [40]. Here, the missing link between contact guidance and an efficient cellular response, (spreading in our case), appears to be linked to the improved stability of focal adhesion that fails to acquire the dynamic state typically characterizing migrating cells (i.e. as it happens for T1). When such interference with focal-adhesion dynamics is not present (i.e. on T2) the contact-guidance effect fully unfolds its potential to enhance endothelial function.

Conclusions

Our data demonstrate a functional link between FA dynamics and cell polarization and spreading on microstructured surfaces presenting variable lateral feature size. We demonstrated that EC mechanotransduction is maximized for specific lateral features, namely for both ridge and groove size of 1 μm. FAs formed by endothelial cells on gratings with low periodicity (T1) were indeed afflicted by a slower turnover and an overall increased stability compared to EC developing on larger gratings (T2), thus possibly inhibiting cell spreading and motility. We believe that these results should be taken into account for the rational design of active surfaces at the interface with the blood stream for regenerative medicine applications.

Acknowledgments

This work was supported in part by the European Union Seventh Framework Programme (FP7/2007e2013) under grant agreement no. NMP4-LA-2009–229289 NanoII and grant agreement no. NMP3-SL-2009–229294 NanoCARD.

References

[1] Dejana E 2004 Endothelial cell-cell junctions: happy together *Nat. Rev. Mol. Cell Biol.* **5** 261–70

[2] Stevens T, Garcia J G, Shasby D M, Bhattacharya J and Malik A B 2000 Mechanisms regulating endothelial cell barrier function *Am. J. Physiol. Lung Cell. Mol. Physiol.* **279** L419–22

[3] Kolaczkowska E and Kubes P 2013 Neutrophil recruitment and function in health and inflammation *Nat. Rev. Immunol.* **13** 159–75

[4] Geiger B, Spatz J P and Bershadsky A D 2009 Environmental sensing through focal adhesions *Nat. Rev. Mol. Cell Biol.* **10** 21–33

[5] Dejana E, Tournier-Lasserve E and Weinstein B M 2009 The control of vascular integrity by endothelial cell junctions: molecular basis and pathological implications *Dev. Cell* **16** 209–21

[6] Schriefl A J, Zeindlinger G, Pierce D M, Regitnig P and Holzapfel G A 2012 Determination of the layer-specific distributed collagen fibre orientations in human thoracic and abdominal aortas and common iliac arteries *J. R. Soc. Interface R. Soc.* **9** 1275–86

[7] Deroanne C F, Lapiere C M and Nusgens B V 2001 *In vitro* tubulogenesis of endothelial cells by relaxation of the coupling extracellular matrix-cytoskeleton *Cardiovasc. Res.* **49** 647–58

[8] Gasiorowski J Z, Liliensiek S J, Russell P, Stephan D A, Nealey P F and Murphy C J 2010 Alterations in gene expression of human vascular endothelial cells associated with nanotopographic cues *Biomaterials* **31** 8882–8

[9] Franco D, Milde F, Klingauf M, Orsenigo F, Dejana E, Poulikakos D, Cecchini M, Koumoutsakos P, Ferrari A and Kurtcuoglu V 2013 Accelerated endothelial wound healing on microstructured substrates under flow *Biomaterials* **34** 1488–97

[10] Franco D, Klingauf M, Bednarzik M, Cecchini M, Kurtcuoglu V, Gobrecht J, Poulikakos D and Ferrari A 2011 Control of initial endothelial spreading by topographic activation of focal adhesion kinase *Soft Matter* **7** 7313

[11] Bettinger C J, Langer R and Borenstein J T 2009 Engineering substrate topography at the micro- and nanoscale to control cell function *Angew. Chem. Int. Edn Engl.* **48** 5406–15

[12] Kanchanawong P, Shtengel G, Pasapera A M, Ramko E B, Davidson M W, Hess H F and Waterman C M 2010 Nanoscale architecture of integrin-based cell adhesions *Nature* **468** 580–4
[13] Pasapera A M, Schneider I C, Rericha E, Schlaepfer D D and Waterman C M 2010 Myosin II activity regulates vinculin recruitment to focal adhesions through FAK-mediated paxillin phosphorylation *J. Cell Biol.* **188** 877–90
[14] Dumbauld D W *et al* 2013 How vinculin regulates force transmission *Proc. Natl Acad. Sci. USA* **110** 9788–93
[15] Dumbauld D W, Michael K E, Hanks S K and García A J 2010 Focal adhesion kinase-dependent regulation of adhesive forces involves vinculin recruitment to focal adhesions *Biol. Cell Auspices Eur. Cell Biol. Organ.* **102** 203–13
[16] Ferrari A, Cecchini M, Dhawan A, Micera S, Tonazzini I, Stabile R, Pisignano D and Beltram F 2011 Nanotopographic control of neuronal polarity *Nano Lett.* **11** 505–11
[17] Balaban N Q *et al* 2001 Force and focal adhesion assembly: a close relationship studied using elastic micropatterned substrates *Nat. Cell Biol.* **3** 466–72
[18] Wozniak M A, Desai R, Solski P A, Der C J and Keely P J 2003 ROCK-generated contractility regulates breast epithelial cell differentiation in response to the physical properties of a 3D collagen matrix *J. Cell Biol.* **163** 583–95
[19] Ferrari A, Cecchini M, Serresi M, Faraci P, Pisignano D and Beltram F 2010 Neuronal polarity selection by topography-induced focal adhesion control *Biomaterials* **31** 4682–94
[20] Ferrari A, Veligodskiy A, Berge U, Lucas M S and Kroschewski R 2008 ROCK-mediated contractility, tight junctions and channels contribute to the conversion of a preapical patch into apical surface during isochoric lumen initiation *J. Cell Sci.* **121** 3649–63
[21] Jacchetti E, Di Rienzo C, Meucci S, Nocchi F, Beltram F and Cecchini M 2014 Wharton's Jelly human mesenchymal stem cell contact guidance by noisy nanotopographies *Sci. Rep.* **4** 3830
[22] Tonazzini I, Meucci S, Faraci P, Beltram F and Cecchini M 2013 Neuronal differentiation on anisotropic substrates and the influence of nanotopographical noise on neurite contact guidance *Biomaterials* **34** 6027–36
[23] Csaderova L, Martines E, Seunarine K, Gadegaard N, Wilkinson C D W and Riehle M O 2010 A biodegradable and biocompatible regular nanopattern for large-scale selective cell growth *Small Weinh. Bergstr. Ger.* **6** 2755–61
[24] Marmaras A, Lendenmann T, Civenni G, Franco D, Poulikakos D, Kurtcuoglu V and Ferrari A 2012 Topography-mediated apical guidance in epidermal wound healing *Soft Matter* **8** 6922
[25] Antonini S *et al* 2014 Human mesenchymal stromal cell enhanced morphological polarization by contact interaction with polyethylene terephthalate nanogratings *Curr. Nanosci.* **10** 773–8
[26] McNamara L E, McMurray R J, Biggs M J P, Kantawong F, Oreffo R O C and Dalby M J 2010 Nanotopographical control of stem cell differentiation *J. Tissue Eng.* 120623
[27] Komatsu R, Ueda M, Naruko T, Kojima A and Becker A E 1998 Neointimal tissue response at sites of coronary stenting in humans: macroscopic, histological, and immunohistochemical analyses *Circulation* **98** 224–33
[28] Park J, Bauer S, Schmuki P and von der Mark K 2009 Narrow window in nanoscale dependent activation of endothelial cell growth and differentiation on TiO_2 nanotube surfaces *Nano Lett.* **9** 3157–64
[29] Lampugnani M G, Corada M, Andriopoulou P, Esser S, Risau W and Dejana E 1997 Cell confluence regulates tyrosine phosphorylation of adherens junction components in endothelial cells *J. Cell Sci.* **110** 2065–77
[30] Meucci S, Tonazzini I, Beltram F and Cecchini M 2012 Biocompatible noisy nanotopographies with specific directionality for controlled anisotropic cell cultures *Soft Matter* **8** 1109
[31] Liliensiek S J, Wood J A, Yong J, Auerbach R, Nealey P F and Murphy C J 2010 Modulation of human vascular endothelial cell behaviors by nanotopographic cues *Biomaterials* **31** 5418–26
[32] Spatz J P and Geiger B 2007 Molecular engineering of cellular environments: cell adhesion to nano-digital surfaces *Methods Cell Biol.* **83** 89–111
[33] Kassis J N, Guancial E A, Doong H, Virador V and Kohn E C 2006 CAIR-1/BAG-3 modulates cell adhesion and migration by downregulating activity of focal adhesion proteins *Exp. Cell Res.* **312** 2962–71
[34] Stevenson N J, McFarlane C, Ong S T, Nahlik K, Kelvin A, Addley M R, Long A, Greaves D R, O'Farrelly C and Johnston J A 2010 Suppressor of cytokine signalling (SOCS) 1 and 3 enhance cell adhesion and inhibit migration towards the chemokine eotaxin/CCL11 *FEBS Lett.* **584** 4469–74
[35] Cavalcanti-Adam E A, Volberg T, Micoulet A, Kessler H, Geiger B and Spatz J P 2007 Cell spreading and focal adhesion dynamics are regulated by spacing of integrin ligands *Biophys. J.* **92** 2964–74
[36] Teo B K K, Wong S T, Lim C K, Kung T Y S, Yap C H, Ramagopal Y, Romer L H and Yim E K F 2013 Nanotopography modulates mechanotransduction of stem cells and induces differentiation through focal adhesion kinase *ACS Nano* **7** 4785–98
[37] Cecchini M, Bumma G, Serresi M and Beltram F 2007 PC12 differentiation on biopolymer nanostructures *Nanotechnology* **18** 505103
[38] Wieringa P, Tonazzini I, Micera S and Cecchini M 2012 Nanotopography induced contact guidance of the F11 cell line during neuronal differentiation: a neuronal model cell line for tissue scaffold development *Nanotechnology* **23** 275102
[39] Ferrari A, Cecchini M, Degl Innocenti R and Beltram F 2009 Directional PC12 cell migration along plastic nanotracks *IEEE Trans. Biomed. Eng.* **56** 2692–6
[40] Ferrari A, Faraci P, Cecchini M and Beltram F 2010 The effect of alternative neuronal differentiation pathways on PC12 cell adhesion and neurite alignment to nanogratings *Biomaterials* **31** 2565–73